

EVALUATION OF MODE SHAPE EXPANSION TECHNIQUES FOR PREDICTION

Marie Levine-West, Mark Mihnan, and Andy Kissil
Jet Propulsion Laboratory, California Institute of Technology,
4800 Oak Grove Drive, M.S. 1S7-316
Pasadena, CA 91109

ABSTRACT

Several methods for mode shape expansion are investigated. In the first, the dynamic equations of motions are used to obtain direct solutions to the expanded eigenvectors. It is shown that these methods can be interpreted as constrained optimization problems. Previously developed methods using orthogonal projections can also be formulated through constrained optimization. To account for uncertainties in the measurements and in the prediction, new expansion techniques based on least squares minimization techniques with quadratic inequality constraints (LSQI) are proposed. These techniques are evaluated with the full set of experimental data obtained on the Micro-Precision Interferometer testbed, using both the pre-test and updated analytical models. The robustness of these methods is verified with respect to measurement noise, model deficiency, number of measured dofs and accelerometer location. It is shown that the proposed LSQI method has the best performance and can reliably predict mode shapes, even in very adverse situations.

NOTATION

a	= measured dofs	= aset dofs
o	= non-measured dofs	= oset dofs
N	= $a + o$	= full set of dofs
p	= number of modes	
\cdot	= notation used for actual test data	
$\hat{\cdot}$	= notation used for expanded test data	
$\omega_i, \tilde{\omega}_i$	= i^{th} analytical / test modal frequencies	
$\phi_{ai}, \tilde{\phi}_{ai}, \hat{\phi}_{ai}$	= $(a \times I)$ i^{th} analytical / test / expanded eigenvector at measured dofs	
$\phi_{oi}, \tilde{\phi}_{oi}, \hat{\phi}_{oi}$	= $(o \times I)$ i^{th} analytical / test / expanded eigenvector at non-measured dofs	
$\Phi_{Np}, \tilde{\Phi}_{Np}, \hat{\Phi}_{Np}$	= $(N \times I)$ matrix of p analytical / test / expanded eigenvectors at full set	
θ_{si}	= strain energy for mode i in element s	
K	= $(N \times N)$ full stiffness matrix	
M	= $(N \times N)$ full mass matrix	
A_{pp}	= $(p \times p)$ unconstrained least-squares projection matrix	
P_{pp}	= $(p \times p)$ orthogonal Procrustes transformation matrix	
$R(X)$	= range of matrix X	
$N(X)$	= null space of matrix X	

1.0 INTRODUCTION

Physical and financial constraints typically limit the number of degrees of freedom (dofs) monitored during a dynamic structural test. These limitations include laboratory or field restrictions, such as available number of accelerometers and/or data channels, structural constraints, such as inaccessibility of certain parts of the structure, or flight project constraints for on-orbit identification. However, it is often desired to assess the modal response of the full structure at all of its dofs. The most common and least demanding reason is for mode shape visualization. Other reasons include correlation of test and analysis results at all the dofs represented in the full Finite Element Method (FEM) model of the structure. Model updating techniques would benefit from the added information provided by mode shapes at all dofs. The full mode shape is also useful in predicting the response at unmeasured dofs for structural integrity and reliability assessments to dynamic loads such as earthquakes, impacts or explosions. Control needs include computation of the strain energy distributions for optimal damper and active member placement in vibration attenuation problems. In addition, the tuning of Multiple Input/ Multiple Output (MI MO) control parameters and gains also benefits greatly from an accurate model at all dofs.

Existing mode shape expansion methods fall into three broad categories, Spatial interpolation techniques use the FEM model geometry to infer the mode shape at unmeasured locations. These methods are very sensitive to spatial discontinuities and are mainly used for plate-like structures such as aircraft wings [9]. Furthermore, the quantity and location of the measured dofs, and pairing of the predicted analytical modes are important factors in the success of this method. The second class of interpolation methods use the FEM model properties, such as mass and stiffness, to obtain a closed-form solution of the mode shapes at unmeasured dofs. These methods include the Guyan static expansion [2], which assumes that the inertial forces at the unmeasured dofs are negligible, and the Kidder dynamic expansion [3] which uses the full dynamic equations to infer the mode shapes at the unmeasured dofs. The third class of interpolation techniques use projection methods to minimize the error between the expanded mode shape and the paired analytical mode shape. This includes the unconstrained least-squares minimization approach proposed by Kammer [7], and the Procrustes method suggested by Smith and Beattie which constrains the projection to be orthogonal [4]. It will be shown that most of these expansion methods can be expressed in terms of a constrained minimization problem. To relax the hard constraints imposed by these methods, and to incorporate the uncertainties in the measurements and in the model, two new mode shape expansion approaches are proposed and investigated herein: penalty methods, and least-squares minimization with quadratic inequality constraints (LSQI).

A study is conducted to evaluate the robustness and reliability of several of these mode shape expansion methods. The methods which are retained for comparison of mathematical and structural performance metrics are the Guyan Static expansion method, the Kidder dynamic method, the Procrustes method, and the new penalty and LSQI methods. Spatial interpolation methods will not be included in the following study since they are not suitable for most structures. Sensitivity studies are performed, using actual experimental data. The studies involve taking a subset of the actual set of instrumented dofs, and verifying the accuracy of the expanded prediction. The methods are evaluated as to their sensitivity to combinations of measurement error, distributed and/or localized modelling errors. Sensitivity to modelling error is evaluated by using both the approximate pre-test finite element model and reconciled updated

model. The performance of the modal expansion techniques is also assessed with respect to sensor location and quantity. It is shown that a new method derived from a least-squares minimization formulation with quadratic inequality constraint provides by far the most reliable mode shape estimates, even in adverse situations.

2.0 MICRO-PRECISION INTERFEROMETER (MPI) TESTBED

The Micro-Precision interferometer (MPI) testbed at the Jet Propulsion Laboratory (JPL) is a lightly-damped truss-structure comprised of two booms and a vertical tower with dimensions of 7m x 6.3m x 5.5111, and weighing 210 kg (The MPI finite element model geometry is shown in Fig. 1). It is composed of 250 aluminum struts connected to 80 node balls. The careful design of the strut to node assembly ensures linearity in the response [5]. The primary objective of the MPI is to perform system integration of Control-Structure Interaction (CSI) technologies to demonstrate the end-to-end operation of a space-based optical interferometer [8]. The high imaging resolution of future space missions will require a 15nm RMS control of the optical pathlength over the 7m baseline of the structure. Accurate modelling and response prediction are essential for the successful implementation of these control methodologies. Detailed modal testing and model updating were performed on the MPI and a high fidelity model was achieved for the first fifteen structural modes up to 60 Hz [5,6]. For the purpose of this analysis, only the first nine structural modes up to 50117 will be considered.

The accuracy of the experimental procedures is substantiated by two independent sets of modal tests, carried out with distinct equipment, processors and personnel. As shown in Table 1, the accuracy of the identified modal frequencies is of the order of 0.5 % and the Modal Assurance Criteria (MAC, (46)) between the two sets of mode shapes is greater than 0.98 for most of the modes. However, the accuracy of the identified mode shapes is only of the order of 15%. This infers that a high degree of uncertainty is associated with mode shape values, even with precise test procedures, excellent frequency repeat ability, and better than average MACS.

Similarly, in Table 11 and Table 111, the pre-test and updated FEM models are compared to the experimental frequencies and mode shapes. These tables show that the original model had frequency errors of the order of 5%, and mode shape errors of the order of 25%, with the largest errors in the higher modes. The model was later improved by a combination of sub-component testing and full model Bayesian estimation [6]. The modal frequencies and mode shape errors were reduced to approximately 1% and 10% respectively, and are within the accuracy expected from the experimental procedure.

These case studies demonstrate that the modal frequency, the MAC and the mass cross-orthogonality (MX, (49)) are quantities that are not very sensitive to experimental errors, modal identification schemes and analytical imprecision. However, mode shape values are, and when predicting mode shapes at unmeasured dofs, it is unreasonable to assume that there is an exact closed-form solution. The following study will investigate methods that take into account existing uncertainties in the measured mode shapes, and will compare these methods to those which assume a closed-form solution exists. It will be shown that the popular closed-form solution methods (the Guyan and Kidder methods) arise from certain variational problems with constraints. Recognizing this, new formulations are proposed and

evaluated based upon relaxing these constraints, thereby taking into account various uncertainties.

3.0 DESCRIPTION OF MODE SHAPE EXPANSION METHODS

In this section several mode shape expansion methods are developed. We begin by showing that the standard Guyan and Kidder expansion techniques are equivalent to certain optimization or variational problems. This new perspective allows us to formulate new methods for mode shape expansion. An extensive comparison of all of these methods will be given in section 5.

3.1. Guyan Static Expansion.

The Guyan static expansion method is based on the assumption that the inertial forces acting on the non-measured dofs can be neglected with respect to the elastic forces [2]. This is accomplished by setting $M_{oo} = M_{oa} = 0$ in the modal force equilibrium equation below:

$$\left(\begin{array}{cc} [K_{aa} & K_{ao}] \\ [K_{oa} & K_{oo}] \end{array} - \omega_i^2 \begin{array}{cc} [M_{aa} & M_{ao}] \\ [M_{oa} & M_{oo}] \end{array} \right) \begin{pmatrix} \phi_{ai} \\ \phi_{oi} \end{pmatrix} = 0 \quad (1)$$

Eq. (1) leads to an exact analytical relationship between the mode shapes at the measured and unmeasured dofs. Using the experimental mode shape data obtained at the instrumented dofs, $\tilde{\phi}_{ai}$, the predicted mode shape at the full set of dofs, $\hat{\phi}_{Ni}$, is obtained as

$$\hat{\phi}_{Ni} = \begin{pmatrix} \phi_{ai} \\ -K_{oo}^{-1} K_{oa} \phi_{ai} \end{pmatrix} \quad (2)$$

An alternate and equivalent formulation results from solving the constrained minimization problem

$$\min_{\hat{\phi}_{Ni}} \frac{1}{2} \langle \hat{\phi}_{Ni}, K \hat{\phi}_{Ni} \rangle \quad \text{subject to } \hat{\phi}_{ai} = \tilde{\phi}_{ai} \quad (3)$$

This problem can be interpreted as finding the expanded mode shape, $\hat{\phi}_{Ni}$, which minimizes the total strain energy of mode i such that the predicted mode shape equals the test values at the measured dofs. It can be demonstrated that the solution to the optimization problem above is given by $\hat{\phi}_{Ni}$ in (2). To see this we first form the Lagrangian $L(x, \lambda)$, where the matrix $E = [I \ 0]$ picks off the observed degrees of freedom (the *aset*), and x is the expanded mode shape of dimension N ,

$$L(x, \lambda) = \frac{1}{2} \langle x, Kx \rangle + \langle \lambda, \tilde{\phi}_{ai} - Ex \rangle. \quad (4)$$

The stationary values of L are the zeros of

$$\frac{\partial L}{\partial x} = \langle Kx, . \rangle - \langle E^T \lambda, . \rangle, \quad (5)$$

and

$$\frac{\partial L}{\partial \lambda} = \langle \hat{\Phi}_{ai} - E x, \cdot \rangle \quad (i)$$

Thus,

$$Kx = E^T \lambda; \quad \hat{\Phi}_{ai} - E x = 0. \quad (7)$$

Under the assumption that there are no rigid body modes,

$$x = K^{-1} E^T \lambda, \quad (8)$$

so that

$$\tilde{\Phi}_{ai} = E K^{-1} E^T \lambda, \quad (9)$$

and consequently

$$\lambda = (E K^{-1} E^T)^{-1} \tilde{\Phi}_{ai}, \quad (10)$$

Substituting the expression for λ above into (8) gives the expanded mode shape x as

$$x = K^{-1} E^T (E K^{-1} E^T)^{-1} \tilde{\Phi}_{ai}, \quad (11)$$

To show that the two mode shape expansions (2) and (11) are identical, we show that the respective static forces leading to these deformations are the same. Taking the mode expansion vector in (2) and multiplying by the partitioned stiffness matrix K (1) leads to the force vector&

$$\begin{aligned} f_g &= K \hat{\Phi}_{Ni} \\ &= \begin{bmatrix} K_{aa} \tilde{\Phi}_{ai} & - K_{ao} K_{oo}^{-1} K_{oo}^T \tilde{\Phi}_{ai} \\ 0 & \end{bmatrix}. \end{aligned} \quad (12)$$

We will next compare f_g with the force vector, f_v , associated with the variational expansion (11). From (11) we find that

$$f_v = E^T (E K^{-1} E^T)^{-1} \tilde{\Phi}_{ai}. \quad (13)$$

Now let $\alpha = E K^{-1} E^T$, so that

$$f_v = \begin{bmatrix} \alpha^{-1} \tilde{\Phi}_{ai} \\ 0 \end{bmatrix} \quad (14)$$

Partitioning K^{-1} as

$$K^{-1} = \begin{bmatrix} \alpha & \beta \\ \beta^T & \delta \end{bmatrix}, \quad (15)$$

we see that

$$\begin{aligned} K_{aa} \alpha + K_{ao} \beta^T &= I, \\ K_{ao}^T \alpha + K_{oo} \beta^T &= 0. \end{aligned} \quad (16)$$

Hence,

$$\begin{aligned} \alpha &= K_{aa}^{-1} [I - K_{ao} \beta^T] \\ &= K_{aa}^{-1} [I + K_{ao} K_{oo}^{-1} K_{ao}^T \alpha] \end{aligned} \quad (17)$$

where α is non-singular, Therefore,

$$a-l = [I + K_{ao} K_{oo}^{-1} K_{ao}^T \alpha]^{-1} K_{aa}, \quad (18)$$

which in turn leads to

$$\alpha^{-1} = K_{aa} - K_{ao} K_{oo}^{-1} K_{ao}^T. \quad (19)$$

From (12), (14) and (19) we see that $\alpha = f_v$.

The interpretation of the static expansion method as an optimization problem serves to motivate the development of several expansion techniques based on the same principle.

3.2. Kidder Dynamic Expansion.

This method was proposed by Kidder [3], and later used by Berman [5] to update structural models. The method is the same as the Gu yan static expansion method except that the inertial forces at the unmeasured degrees of freedom are no longer assumed to be negligible. An analytic expression of the mode shapes at the unmeasured dofs, $\hat{\phi}_{oi}$, as a function of the test modal frequency, $\hat{\omega}_i$, and the test mode shapes at the measured dofs, $\hat{\phi}_{ai}$ can again be realized:

$$\hat{\phi}_{Ni} = \begin{bmatrix} \tilde{\phi}_{ai} \\ (K_{oo} - \hat{\omega}_i^2 M_{oo})^{-1} (K_{oa} - \hat{\omega}_i^2 M_{oa}) \tilde{\phi}_{ai} \end{bmatrix} \quad (20)$$

As with the Guyan expansion method, there is a variational principle from which to derive the Kidder expansion above. To begin we let S denote the surface in \mathbf{R}^N ,

$$S = \{ (\tilde{\phi}_{ai}, w): w \in \mathbf{R}^{N-a} \}, \quad (21)$$

where $\tilde{\phi}_{ai}$ denotes the partially *observed* i^{th} modal vector at a dofs, We seek solutions of the dynamical system constrained to S . By D'Alembert's principle any motion $y(t) \in S$ satisfies

$$\langle M \ddot{y} + Ky, \xi \rangle = 0, \quad (22)$$

for all vectors ξ tangent to S . Each such ξ can be realized as

$$\xi = Fw,$$

where $w \in \mathbf{R}^{N-a}$ and

$$F = \begin{bmatrix} \mathbf{0}_{a \times (N-a)} \\ \mathbf{I}_{(N-a) \times (N-a)} \end{bmatrix} \quad (24)$$

At the observed resonance

$$y(t) = \begin{bmatrix} \hat{\Phi}_{ai} \\ \Phi_{oi} \end{bmatrix} \sin \hat{\omega}_i t, \quad (2s)$$

where $\hat{\omega}_i$ denotes the observed frequency. Eq. (22)--(25) then imply that

$$\langle K \phi - \hat{\omega}_i^2 M \phi, F w \rangle = 0 \quad \text{for all } w \in \mathbb{R}^{N-a}, \quad (26)$$

with

$$\phi = \begin{bmatrix} \hat{\Phi}_{ai} \\ \Phi_{oi} \end{bmatrix}. \quad (27)$$

Therefore,

$$F^T [K - \hat{\omega}_i^2 M] \phi = 0,$$

or equivalently

$$K_{ao} \hat{\Phi}_{ai} - \hat{\omega}_i^2 M_{ao} \hat{\Phi}_{ai} + K_{oo} \Phi_{oi} - \hat{\omega}_i^2 M_{oo} \Phi_{oi} = 0. \quad (28)$$

From this we obtain the expansion at the unmeasured degrees of freedom as

$$\hat{\Phi}_{oi} = [K_{oo} - \hat{\omega}_i^2 M_{oo}]^{-1} [\hat{\omega}_i^2 M_{oa} - K_{oa}] \hat{\Phi}_{ai} \quad (29)$$

in accordance with (20).

The ‘‘Kidder Dynamic Expansion’’ method described herein is not to be confused with the ‘‘Dynamic Expansion Method’’ proposed by O’Callaghan [10], The latter adds a dynamic force correction term to the Guyan expanded result which is expressed in terms of both the full FEM model, M and K , and the Guyan reduced FEM model at the observed dofs, m_a and k_a :

$$\hat{\Phi}_{fi} = K_{oo}^{-1} K_{oa} \hat{\Phi}_{ai} + K_{oo}^{-1} [M_{oa} - M_{oo} K_{oo}^{-1} K_{oa}] m_a^{-1} k_a \hat{\Phi}_{ai} \quad (30)$$

The dynamic expansion method has been shown to produce reasonable results on actual test cases [11], although it is sensitive to test and analysis errors [12]. However, it is based on a series of equation manipulations which we unfortunately could not relate to a particular physical interpretation. The same remark applies to the ‘‘Hybrid Expansion’’ method proposed by Kammer [13], We will restrict our attention to those methods that we have derived from a variational principle, and will not consider these two particular methods any further.

3.3 Least-Squares Projection Methods.

Both the Guyan and Kidder expansion methods require an *a priori* knowledge of the FEM mass and stiffness matrices to predict mode shapes at unmeasured degrees of freedom. Kammer [7], and later O'Callaghan [14] and Lallement [15] have proposed methods which only require *a priori* knowledge of the analytical mode shapes. These methods determine a transformation A_{pp} that minimizes the quadratic error between the experimental and analytical mode shapes at the measured dofs. The method is also known as the "Modal Expansion" method. The transformation is used with the full analytical mode shapes to infer the experimental mode shapes at the unmeasured degrees of freedom. The transformation A_{pp} is computed from the p measured modes and paired analytical modes from the unconstrained minimization problem:

$$\min_{A_{pp}} \|\hat{\Phi}_{ap} - \Phi_{ap} A_{pp}\|_F^2, \quad (31)$$

where $\|\cdot\|_F$ denotes the Frobenius norm of a matrix,

$$\|X\|_F^2 = \text{tr}(X^T X); \quad \text{tr} = \text{trace operator}. \quad (32)$$

The minimization problem (31) above has a unique solution only if the number of measured dofs exceeds the number of modes, and $\hat{\Phi}_{ap}$ has full column rank p . Under those conditions, the matrix A_{pp} is obtained via the Moore-Penrose pseudo-inverse, A_{pp} is then used to compute the expanded mode shapes from the p measured modes and paired analytical modes. A variation of this method is also possible, where the expanded dofs are constrained to match the experimental values at the measured dofs.

The second method, the "Procrustes Expansion Method" is a variation of the first in which the transformation A_{pp} is required to be orthogonal. This method expands the mode shapes by orthogonal Procrustes transformation of the experimental eigenvectors into the space spanned by the predicted analytical eigenvectors at the measured dofs [4]:

$$\min_{P_{pp}} \|\hat{\Phi}_{ap} - \Phi_{ap} P_{pp}\|_F^2 \quad \text{subject to} \quad P_{pp}^T P_{pp} = I. \quad (33)$$

The orthogonality constraint has the geometric interpretation of finding the best fitting "rotation" of the analytical to experimental data. The mode is then extrapolated to the unmeasured degrees of freedom by this same rotation. Other variations of this technique are discussed in [4].

3.4. Penalty Methods.

In this section we will relax the equality constraints by replacing them with a penalty term. This will be done for both the Guyan and Kidder expansion methods. For the Guyan method this is a pure penalty term; for the Kidder expansion a potential energy terms that serves to drive the system trajectory to the surface S defined in (21) is added to the Lagrangian of the mechanical system. The introduction of a penalty term is just one way to relax the hard constraint. A different approach to relaxing the constraint will be discussed in the following section.

The constrained minimization version of the Guyan expansion method imposes that the value of the expanded mode shape at the measured dofs identically equal the measured values. These measured values are typically contaminated with error. Furthermore, these existing errors in the experimental values propagate errors in the estimates of the mode shape at the unmeasured dofs. To take into account the

uncertainty in the measured mode shapes, penalty methods are applied in the Guyan expansion case to minimize a weighted sum of the modal strain energy and the error in the measured mode shape. The unconstrained minimization problem with measurement error penalty is

$$\min_{\hat{\phi}_{Ni}} \frac{1}{2} \langle \hat{\phi}_{Ni}, K \hat{\phi}_{Ni} \rangle + \frac{1}{2} \gamma \left| \hat{\phi}_{ai} - E \hat{\phi}_{Ni} \right|^2, \quad (34)$$

where γ is a scalar that weights the contribution of the "soft constraint" $E \hat{\phi}_{Ni} = \tilde{\phi}_{ai}$. The solution to this problem is easily computed as

$$\hat{\phi}_{Ni} = \gamma [K + \gamma E^T E]^{-1} E^T \tilde{\phi}_{ai}. \quad (35)$$

Using the partitioned form for K in (15), it is straightforward to verify that as $\gamma \rightarrow \infty$, the expanded eigenvector is constrained to match the experimental values at the measured dofs, and the solution converges to that of the Guyan method in (2).

The analogous penalty method formulation for the Kidder method is developed by modifying the potential energy of the Lagrangian with an additional term $V(y)$ in (22) of the form

$$V(y) = \min_{m \in S} |y - m|^2, \quad (36)$$

where S is the manifold defined in (21). Thus we write

$$L = \langle M \dot{y}, \dot{y} \rangle + \langle K y, y \rangle + \gamma V(y). \quad (37)$$

Again assuming that $y(t) = \sin \tilde{\omega}_i t$, and noting that $V(y) = |E x - \tilde{\phi}_{ai}|^2$, we find using d'Alembert's principle that

$$\hat{\phi}_{Ni} = \gamma \left[\tilde{\omega}_i^2 M - K - \gamma E^T E \right]^{-1} E^T \tilde{\phi}_{ai} \quad (38)$$

As with the penalty version of the Guyan method, it can be shown that as $\gamma \rightarrow \infty$, the solution above converges to the solution (20).

Penalty methods use the weighting variable γ as a measure of the relative confidence in the measured mode shape. This problem is analogous to that of the generalized least squares method in which the variable γ can be interpreted as the inverse covariance due to measurement error, assuming that the errors are uncorrelated and identical at all measured dofs. In reality, it is difficult to quantify the variance of such errors. The best value of γ can be evaluated by minimizing the error between the predicted expanded mode shape and the actual measured mode shapes at all dofs. This of course cannot be done in practice. Depending on the mode number, the number of measured locations, and the number of expanded locations, the best value for γ varies between 10^5 and 10^9 for this particular data set. A typical sensitivity plot of γ as a function of mode shape error is shown for several modes in Fig. 2 in which the optimum values are marked. It is seen that acceptable values of the weighting parameters γ can be selected within an order of magnitude about the optimal values.

The ratio of the total strain energy to the weighted mode shape error is shown in Fig. 3 as a function of the weighting parameter γ . The optimal γ 's, represented by a dot, are found to be in the slope transition region between dominant strain energy and dominant mode shape error. This observation still holds when noise is analytically added to the measured data to simulate poor quality data. In practice an

optimal value of γ can never be established, and it is proposed to use the magnitude order of the slope transition region as an approximation to the penalty weighting coefficient.

A variation of the penalty formulation is to use the mode shape obtained from one of the direct expansion methods, instead of the measured mode $\tilde{\phi}_{ai}$ in the formulation (34). Direct expansion methods are those that have a closed-form solution, such as the Guyan static and the Kidder dynamic methods (cf (2), (20)). Denoting the Guyan expanded mode as $\hat{\phi}_{Ni}^d$, the resulting solution for the unconstrained minimization of the modal strain energy with expansion error penalty is

$$\hat{\phi}_{Ni} = \gamma [K + \gamma I]^{-1} \hat{\phi}_{Ni}^d. \quad (39)$$

Note that $\hat{\phi}_{Ni} \rightarrow \hat{\phi}_{Ni}^d$ as $\gamma \rightarrow \infty$. A similar variation can be formulated for the penalty counterpart of the Kidder method from (38).

3.4. Least-Squares with Quadratic Inequality Constraints.

The constrained minimization versions of the Guyan and Kidder expansion methods impose that the value of the expanded mode shape at the measured dofs, $\hat{\phi}_{ai}$, identically equals the measured values $\tilde{\phi}_{ai}$. Relaxing these hard constraints can accommodate for measurement error, leading to a smoother and more robust expansion of the modes. In the previous section we developed a penalty method approach. In this section we pursue an alternate formulation for replacing the hard constraints by a least-squares problem with quadratic inequality constraint (LSQI). The general form of this problem is

$$\min_{\phi} |A\phi - b|^2 \quad \text{subject to} \quad |B\phi - d|^2 \leq \alpha |\phi|^2. \quad (40)$$

The immediate advantage of the LSQI formulation is to allow convergence within a domain of probable solutions, while taking into account uncertainties associated with experimental errors. Mathematical techniques for solving this problem **have been published and are easily implemented** [1]. A computationally efficient implementation exploiting the fact that the number of measured dofs is typically much smaller than the number of total model dofs will be derived in section 6. Using the template defined by (40), three different modal expansion methods are investigated hereby varying the matrix and vector parameters A, B, b , and d .

The first of these is the “Least-Squares Strain Energy Minimization with Quadratic Measurement Error Inequality Constraint”, LSQI 1. This is the counterpart of the constrained optimization form of the Guyan method defined in (3). It finds the expanded mode shapes which minimize the modal strain energy, under the provision that the quadratic mode shape error at the measured dofs is of the order of the experimental uncertainty. Using the fact that the stiffness $K \in \mathbb{R}^{N \times N}$ is a symmetric positive definite matrix, there exists a unique upper triangular matrix $G \in \mathbb{R}^{N \times N}$ (e.g., Choleski factorization), such that:

$$K = G^T * G$$

Hence, the LSQI1 problem is expressed as:

$$\min_{\hat{\phi}_{Ni}} G \hat{\phi}_{Ni}^2 \quad \text{subject to} \quad |\hat{\phi}_{ai} - \tilde{\phi}_{ai}|^2 \leq \alpha \tilde{\phi}_{ai}^2.$$

Or equivalently,

$$\min_{\hat{\phi}_{Ni}} \langle K \hat{\phi}_{Ni}, \hat{\phi}_{Ni} \rangle \quad \text{subject to} \quad |E \hat{\phi}_{Ni} - \tilde{\phi}_{ai}|^2 \leq \alpha |\tilde{\phi}_{ai}|^2. \quad (41)$$

As $\alpha \rightarrow 0$, LSQ11 converges to the Guyan static expansion in (2). Based on the results obtained from the two independent sets of experimental data mentioned previously, a nominal value of 15% is assumed for the expected mode shape error parameter α used in the LSQ1 expansion methods. Sensitivity of the LSQ1 methods to values of α will be discussed.

The second of these methods is the "Least Squares Strain Energy Minimization with Quadratic Expansion Error Inequality Constraint", LSQ12. Here again the modal strain energy is minimized, but subject to the constraint that the quadratic error between the optimally expanded mode shape, $\hat{\phi}_{Ni}$, and the mode shape obtained from direct expansion, $\hat{\phi}_{Ni}^d$, is less than the expected experimental error. LSQ12 is formulated as

$$\min_{\hat{\phi}_{Ni}} \langle K \hat{\phi}_{Ni}, \hat{\phi}_{Ni} \rangle \quad \text{subject to} \quad |\hat{\phi}_{Ni} - \hat{\phi}_{Ni}^d|^2 \leq \alpha |\tilde{\phi}_{ai}|^2. \quad (42)$$

As $\alpha \rightarrow 0$, LSQ12 converges to the direct expansion solution $\hat{\phi}_{Ni}^d$.

The third formulation is the "Least Squares Dynamic Residual Force Minimization with Quadratic Measurement Error Inequality Constraint", LSQ13. In this formulation the objective function is defined as the quadratic norm of the modal "residual force. The LSQ1 problem is now to find the optimal $\hat{\phi}_{Ni}$ that minimizes the modal residual force such that the quadratic error between the expanded mode shape and the experimental mode shape at the measured dofs is within the bounds expected from experimental error,

$$\min_{\hat{\phi}_{Ni}} |(K - \tilde{\omega}_i M) \hat{\phi}_{Ni}|^2 \quad \text{subject to} \quad |E \hat{\phi}_{Ni} - \tilde{\phi}_{ai}|^2 \leq \alpha |\tilde{\phi}_{ai}|^2. \quad (43)$$

As $\alpha \rightarrow 0$, LSQ13 indirectly solves the eigenvalue problem for the given experimental modal frequency and mode shape data at the measured dofs.

4.0 PERFORMANCE METRICS.

Several metrics are used to evaluate the error of a predicted measure σ with respect to a reference measure σ . The first error metric proposed evaluates the relative quadratic point-to-point error at each dof between the predicted expanded mode shape $\hat{\phi}_{Ni}$ and the actual measured mode shape $\tilde{\phi}_{Ni}$, for each mode i :

$$\Delta(i) = \frac{|\hat{\phi}_{Ni} - \tilde{\phi}_{Ni}|}{|\hat{\phi}_{Ni}|}. \quad (44)$$

In comparing mode shapes at each point, normalization of the eigenvectors is achieved by a least squares fit of the expanded mode shape to the reference mode shape via

$$\hat{\phi}^{LS_{Ni}} = P \hat{\phi}_{Ni}, \quad \rho = \frac{\langle \hat{\phi}_{N/i} \hat{\phi}_{Ni} \rangle}{\langle \hat{\phi}_{N/i} \hat{\phi}_{N/i} \rangle}$$

Alternatively, the mean cumulative error in the mode shape as a function of the n^{th} mode can be used to determine the modal number at which the expansion methods start to break down :

$$C(n) = \frac{1}{n} \sum_{i=1}^n A(i). \quad (45)$$

The orthogonality properties of eigenvectors, as inferred in the Modal Assurance Criteria (MAC), can also be used as a performance metric. The MAC matrix between two eigenvectors ϕ_i and ϕ_j is defined as

$$MAC_{ij} = \frac{|\phi_i^T \phi_j|^2}{|\phi_i^T \phi_i| |\phi_j^T \phi_j|}. \quad (46)$$

The MAC is used here to verify the orthogonality between the expanded mode shapes and the actual mode shapes measured at all dofs. From (46) we see that the ideal MAC matrix is the identity matrix.

It is relatively straightforward to establish a relationship between the MAC and normalized norm squared difference between eigenvectors as in (44). To show this relationship, assume ϕ and ψ are two unit vectors, By orthogonal projection we can write

$$\psi = \beta \phi + \epsilon,$$

where β is a scalar and $\langle \epsilon, \phi \rangle = 0$. Now note that $|\beta \phi + \epsilon|^2 = 1$ implies that for small ϵ ,

$$\beta \approx 1 - \frac{|\epsilon|^2}{2}.$$

Hence,

$$MAC_{\phi\psi} \approx 1 - |\epsilon|^2.$$

On the other hand, we have

$$\begin{aligned} |\phi - \psi|^2 &= |(\beta - 1)\phi + \epsilon|^2 \\ &= (\beta - 1)^2 + |\epsilon|^2 \\ &\approx |\epsilon|^2. \end{aligned}$$

Thus,

$$|\phi - \psi| \approx |\epsilon|. \quad (48)$$

Comparing (47) and (48) we see, for example, that a norm difference of 10% between two vectors is equivalent of approximately .99. Thus the norm error appears to be a significantly more sensitive measure of performance than the MAC.

A third performance metric uses global mass properties and is based on the mass cross-orthogonality (MX) of structural eigenvectors. The MX matrix between two eigenvectors, ϕ_i and ϕ_j is defined as

$$MX_{ij} = \langle \phi_{Ni}, M \phi_{Nj} \rangle . \quad (49)$$

in this study MX is used to measure the mass cross-orthogonality of the expanded experimental mode shape with respect to the full experimental mode shape. If ϕ_i and ϕ_j are mass orthogonal, then MX is a diagonal matrix. Furthermore, if ϕ_i and ϕ_j are mass normalized, then MX is the identity matrix.

The three performance metrics discussed above are global metrics describing the total error throughout the whole set of dofs. Errors can also be evaluated at the local structural element level by the strain energy distribution associated with each elements and with each mode i . Analogous to MX which measures the accuracy of the expanded mode shape with respect to the FEM mass matrix M , the element modal strain energy verifies the fit of $\hat{\phi}_{Ni}$ with respect to the FEM stiffness matrix K . In the following definition, k_{ss} is the element stiffness, and $\hat{\phi}_{si}$ is the i^{th} expanded mode shape at the element dofs s , and $\hat{\theta}_{si}$ is the element modal strain energy. $\hat{\theta}_{si}$ is normalized with respect to the total strain energy for that mode ,

$$\hat{\theta}_{si} = \frac{k_{ss} \langle \hat{\phi}_{si}, \hat{\phi}_{si} \rangle}{\langle K \hat{\phi}_{Ni}, \hat{\phi}_{Ni} \rangle} . \quad (50)$$

The element strain energy error between the analytical θ_{Ni} and the expanded $\hat{\theta}_{si}$ identifies the discrete dofs where the expansion does not agree with the mode]. Such errors typically result from localized modelling errors or actual structural damage.

s.0. SENSITIVITY STUDY OF IUWANSION METHODS.

This section will compare the expansion methods outlined in Section 3 with respect to the performance metrics defined in the previous section. Several deviations from an “ideal” data set will be considered. These include added noise in the measurements, the use of different size data sets and locations of measured degrees of freedom, inadequacy of the *a priori* model, and finally combinations of model form error and measurement error.

S.1. Expansion performance with respect to nominal data and updated FEM model.

The expansion methods are first investigated for their reliability and intrinsic performance when all experimental and analytical conditions are “ideal”. The expansion is executed with the updated (i.e., “ideal”) FEM model and mode shapes from a subset of the high quality experimental data measured on the MPI testbed. The measured data is not corrupted by additional noise. Here, twelve locations have been retained as the “measured” set, and are expanded to the full 240 dofs recorded during the actual test. The final 240 dof locations represent 3 dofs at each of the 80 node balls forming the truss structure. The location of the 12 dofs are optimally selected to give for a Guyan reduced model the best MAC with respect to the predicted analytical modes. This particular set of instrument locations is referred to as *aset 5*. As will be demonstrated through the test cases, *aset 5* provides enough information to identify the first nine modes, with the exception of mode 6, which is not exhibited at all. The expansion of missing mode 6 will thus provide a measure of each method’s robustness to unmeasured modal information.

The methods compared in this survey are: (i) Guyan (2), (ii) Kidder (20), (iii) Procrustes (33), (iv) Modal strain energy minimization with measurement error or Kidder expansion error, PEN1 (35) and PEN2 (39), respectively, (v) LSQI with measurement error (LSQI1, (41)), LSQ1 with expansion error (LSQI2, (42)), and LSQI with residual dynamic force minimization, (LSQI3, 43)).

The MAC of the mode shapes expanded from experimental *aset 5* data (12 dofs) with respect to the actual full measurements (240 dofs) is shown in Fig. 4 for all eight expansion methods. The MAC of the ideal analytical model with respect to the full 240 dofs measurement set is also included in Fig. 4 for reference. The Guyan method expands the first 2 modes properly with MAC's greater than .98. However, modes 3 through 5 are poorly correlated, and modes 6 through 9 are not represented at all. PEN1 yields expanded mode shapes which have the same level of accuracy as the Guyan expansion. LSQI1 produces mode shape estimates which are slightly worse than the Guyan method, especially in the lower modes. The Kidder method generates expanded mode shapes which have MAC's greater than .97 for seven of the nine modes. Mode 9 has a MAC of .90, and mode 6 could not be identified at all since it was not represented in the measurement set. Again, the PEN2 and LSQI2 yield the same level of accuracy as the Kidder expansion.

The Procrustes expansion method can predict mode 6, and produces MAC's greater than .85 for all nine modes. However, only modes 1 and 3 are greater than .95. The mediocre results are explained by the fact that all nine modes are expanded simultaneously from the initial 12 dof subset. In Section 5.2 it is shown that the Procrustes method is very sensitive to the number of simultaneously expanded modes and to the set of measurement locations.

Of all the expansion methods, LSQI3 is the one that performs the best across all modes. It is capable of predicting unmeasured mode 6 better than the Procrustes method. Foremost, it is the **only expansion method investigated so far which results in better MAC diagonals** with respect to the measured data than the analytical model used to expand the modes.

The observations made on the performance of the expansion methods with respect to the MAC also hold for the mode shape Frobenius norm error (Fig. 5) and for the mass cross-orthogonality condition (Fig. 6).

5.2. Sensitivity to Mode Shape Measurement Errors.

Noise in the measured mode data can become an important factor, especially when the expanded mode is used in strain energy computations for active member placement. Mode shape noise is still important, but to a lesser degree, when the extrapolated mode is used for computing elastic forces as is done in satisfying the modal force equilibrium equation to update FEM models. There are many sources of noise in the processing of mode shapes. Accelerometers, wires, and the method of data acquisition (i. e., number of averages, etc.). When transfer functions are processed to identify the mode shapes, an additional error can be introduced by the method of eigenvector computation (curvefitting, least squares,...). It suffices to say that the measured mode is never pristine. It is desirable, therefore, to have a mode shape extrapolation procedure that is not only insensitive to noise, but that can filter it out as well.

A sensitivity analysis is performed herein to evaluate the performance of the mode shape extrapolation methods with respect to distributed measurement noise. For these investigations the noise is represented

as an additive Gaussian random error superimposed upon the true mode shape. Spatially localized errors will be considered later in the context of isolated modeling errors and damage.

The Frobenius norm difference between the mode shapes obtained from the two independent tests were of the order of 15%. This level serves as a basis for the following error analysis. The performance of the expansion methods consider the effect of mode shape errors of the order 15%, 25%, and 50%. Errors of the order of 50% are considered representative of gross experimental error, such as noisy or malfunctioning instrumentation, poor experimental procedures, or deficient modal estimation schemes. To infer the mean prediction, Monte Carlo simulations are performed with 30 averages. The analysis reveals that the penalty methods and the LSQI methods with strain energy minimization provide at a very high computational cost only a minor improvement in the predicted expansion compared to the Guyan or Kidder methods. The following performance evaluation will thus be limited to the Guyan, Kidder, Procrustes and LSQI3 methods.

The Frobenius norm error between the expanded and fully measured mode shapes is compared for the first nine modes of the MPI. The expansion is from *aset 5* with 12 dofs up to the full 240 dofs, and is achieved with the updated “ideal” FEM model and eigenproperties. The results are summarized in Figure 7, where the mean expansion error over the first nine mode shapes is plotted as a function of noise level for each of the expansion methods. The error between the “ideal” analytical mode shapes and the measured mode shapes at all dofs with and without added measurement noise are included for comparison.

As expected the performance of the expansion methods grows worse as the noise in the measured data increases. As before, the Guyan method has the overall worst performance, followed by the Kidder and the Procrustes methods. The Kidder method is the most sensitive and exhibits linear growth in the mode shape error as a function of measurement error. The Guyan, Procrustes and LSQI3 methods are equally sensitive to measurement noise, and a 15% noise level does not significantly increase the error in the expanded mode shape for any of these methods. Only when the noise level reaches 25% do differences start to appear. As in the ideal situation, the error in the modes expanded with the Guyan, Kidder, and Procrustes methods are greater or equal than the error in the measurement. Only the LSQI3 method is capable of expanding mode shapes to a greater level of accuracy than the measured data, even when the original data is corrupted by significant amounts of noise. In fact, for moderate amounts of measurement noise, e.g., less than 25%, the first nine modes expanded with the LSQI3 method from 12 instrument locations to the full 240 dofs are almost as accurate as the noise-free mode shapes measured at all dofs. These remarks are consistent with other performance metrics, as shown in Fig. 8 representing the matrix norm error of the MAC for the first nine modes. The error is a measure of the projection of the set of expanded eigenvectors into the space of measured eigenvectors, and includes both the diagonal and off-diagonal terms. Although the Procrustes method constructs the mode shape through an orthogonal projection, the LSQI3 method achieves better orthogonality with respect to the actual data set.

s.3. Sensitivity to selection of number of dofs and their location.

Five different sets of instrument locations and number of dofs are considered, i.e., *aset* 's, as summarized in Table V. The data measured at the a set location are expanded to the full 240 dofs, representing an expansion ratio of 1 to 80 for *aset 1*, 1 to 40 for *aset 2* and *aset 3*, and 1 to 20 for *aset*

4 and *aset 5*. The instrument location is selected either according to engineering judgement at the dofs of highest deformation, i.e. the tip of the booms, or according to optimality criteria such as best MAC fit from a static reduction or best mode shape fit over multiple modes.

The mean mode shape errors of the first nine modes (ϵ from (45)) are summarized in Fig. 9 for each expansion method as a function of the *aset* selection. As expected the expansion error decreases as the number of instrumented locations increase. Again, the Guyan method has the worst performance over all cases, Procrustes is the most sensitive to the *aset* selection, as shown by the 75% decrease in error from *aset 1* to *aset 5*. The large errors for *aset 1*, *aset 2*, and *aset 3* are to be expected, since the Procrustes method requires at least as many measured dofs as modes to uniquely accomplish the orthogonal projection. Expansion with the Kidder method only benefits slightly by an increase in the number of dofs. As before only the LSQ13 method is capable of expanding the mode shape to the same degree of accuracy as the measured data, regardless of the selected *aset*. Fig. 9 also shows the sensitivity of the expansion error to dof location, *Aset 2* and *aset 3* include the same number of dofs, but located at different points on the structure. Whereas the performance of the Kidder method improved from *aset 2* to *aset 3*, the Procrustes method worsened. This implies that for optimal performance, each expansion method should have its own set of dof selection criteria.

A separate analysis demonstrates that the Procrustes method is not only sensitive to the *aset* selection, but also to the number of modes used in the simultaneous expansion and to the pairing between the analytical and experimental modes. This is a disadvantage compared to the Guyan, Kidder and LSQ13 methods which expand the modes individually without the need for mode pairing. In these latter methods the mode pairing is indirectly accomplished through the FEM mode] and does not require any user input or engineering judgement. For the purpose of this analysis, the error in the expanded mode shapes are investigated for two alternate implementations of the Procrustes method. In the first method modes 1 through 9 are expanded *simultaneously* using the first nine analytical modes, irrespective of the number of dofs. in the second approach, the n^{th} mode is expanded from the set formed by the first n analytical modes, disregarding the higher modes. This is referred to as the incremental form of the Procrustes method. Fig. 10 shows the mean cumulative mode shape error for each of the methods from *aset 3* (6 dofs) to the full 240 dofs using the first nine modes. It is seen how, as expected, the Simultaneous Procrustes has a poor performance, especially at the lower modes, since the number of expanded modes (i. e., 9) exceeds the number of measured dofs (i. e., 6). Whereas the Incremental Procrustes has a good performance similar to the Kidder and the LSQ1 methods up to mode 5. However, beyond mode 5 the performance of the Incremental Procrustes deteriorates rapidly since the number of modes exceeds the number of measured dofs. Thus, for this particular *aset* selection the Procrustes method can only simultaneously expand the first five modes with accuracy from the six measured dofs to the full 240 dofs.

The same analysis is performed for the expansion from *aset 5* (12 dofs) to 240 dofs, which includes twice as many measured locations as *aset 3* (Fig. 11). The degrees of freedom in *aset 5* are located to provide the best orthogonality over the first nine modes using a Guyan reduction in the analytical model. The main effect of *aset 5* is to improve the accuracy of the Guyan and Simultaneous Procrustes methods, especially in the lower modes for which the error is reduced by 80%. With *aset 5* both Procrustes methods also converge towards a lower expansion error beyond the fifth mode. Again, the *aset* location criteria is a major factor in the reliability of the Procrustes method, and method specific

criteria must be devised to improve the performance.

S.4, Sensitivity to Model Error.

All the modal expansion methods proposed herein use an analytical model to predict the mode shapes at the unmeasured dofs. The FEM model plays an important role in the regularization of spurious information, the filtering out of the measurement error, and the prediction in the event of insufficient information. This is especially true of the Kidder and the LSQI3 methods which rely heavily on the full dynamic equations. In the following, both distributed (*i.e.*, global), and localized errors are investigated.

Distributed errors in the analytical mass or stiffness matrix, such as errors resulting from the uniform structural properties (e.g., mass density or modulus of elasticity), only scale the eigenvalue problem by a multiplicative constant. Thus there is no change to the analytical eigenvectors, and consequently, distributed property errors in the model have little influence on modal expansion prediction,

Another form of global model error can be introduced by deficiencies in the model form, as would typically occur in a pre-test model. To this effect the actual pre-test model of the MPI is used for demonstration. It is composed uniquely of rod elements, and can only predict the first 4 modes. The “ideal” updated model is constructed uniquely of bar elements, and can accurately predict the first nine modes. As shown in Fig. 12, the mean cumulative mode shape error over nine modes is 20% for the pre-test model, and is only 10% for the updated model, which is below the experimental inaccuracies. The errors in the Guyan, the Kidder, the Procrustes, and the LSQI3 methods expanded with the pre-test model from *aset 5* to the full 240 dofs are also shown in Fig. 12. As expected, the level of error is slightly worse when the eigenvectors are expanded with the pre-test model than with the updated model, especially in the higher modes where the pre-test and updated model start to diverge (see Fig. 11). The Guyan and the Procrustes methods display little sensitivity to model form error. The Kidder method is the most sensitive, as is shown by the sharp increase in the error beyond mode 3 resulting in a mean error which is twice as high than that obtained with the updated model expansion. Although the performance of LSQI3 has also worsened, it is still the best by a factor of two relative to the other expansion methods, and it remains the only method which is capable of expanding mode shapes to a higher degree of accuracy than the model.

Spatially localized model error, such as would occur from local errors in the model form or properties, or from changes in the actual structure resulting from fatigue or damage are also expected to affect the predictability of the expanded mode shapes. To simulate this situation the stiffness of the longest strut in the pre-test model, connecting the tower to the optics boom, is decreased by half. This only changes the pre-test frequencies of modes 5 and 6 by less than 3%, while keeping all other frequencies almost the same. However, the effect of this localized error on the analytical mode shapes is significant, as shown in Fig. 13 where a major jump between modes 5 and 6 corresponds to a 300% increase in the mode shape error relative to the “undamaged” pre-test model. All other mode shapes remain virtually unchanged. Although the effect on the analytical modes is extreme, none of the expanded mode shapes are affected, and the expansion errors for each method is almost the same as those obtained previously with the “undamaged” pre-test model (Fig. 12). The fact that the expansion error does not

increase from the “undamaged” pre-test model case implies that the expansion errors are more sensitive to global mode] form errors than to localized element errors.

The expanded mode shapes obtained here with the LSQI3 method are used to compute the element strain energy as defined in (50). When compared to the element strain energy predicted analytically by the “damaged” model, the largest differences occur in the “damaged” member. Thus, LSQI3 is capable of expanding mode shapes to the accuracy required to identify faulty elements in the model.

5.5. Sensitivity to measurement and model error.

Finally, to assess the performance of the expansion methods to a combination of modeling and measurement error, the last case with the model form error and the localized model error was repeated with an additional 25% error in the measured mode shape values. The results are summarized in Fig. 14. **The solid lines represent the accuracy of the different forms of the MPI model with respect to the true test data at all dofs, and the dashed lines represent the expanded mode shapes from aset 5 to the full 240 dofs using the damaged pre--test model and noise corrupted measurements.**

As expected, adding measurement noise to the damaged pre--test model worsened the performance of all the expansion methods by approximately 50% (Figs. 13--14). In the presence of both model error and measurement noise, the Guyan and Kidder method perform equally poorly, and generate mode shapes which are worse than predicted by the damaged pre-test model. The Procrustes method performs better than the Guyan and the Kidder methods, especially at the higher modes, and can predict the lower modes to the same level of accuracy as the noise contaminated data. Once again the LSQI3 method performs exceptionally well. It generates mode shapes which are only off by 15%, although the data **used is contaminated by 25% noise and the model has the wrong form and a damaged member.** Furthermore, comparison between the element strain energies of the damaged pre--test model and LSQI3 expanded mode **shapes show that the largest differences** occur at the “damaged” strut location. Thus, the mode shapes expanded with the LSQI3 method are capable of identifying damage or localize model error, even in the presence of measurement noise.

6. EFFICIENT LSQI3 ALGORITHM.

Standard solution techniques for the LSQI method (43) involve a generalized singular value decomposition of the full $N \times N$ dynamic force matrix and the $N \times I$ partitioning matrix E , which require $O(N^3)$ operations. This can become prohibitively large when expanding modes of structures with over 1000 dofs. A new LSQI algorithm is proposed, which takes advantage of the fact that the number of measured dofs, u , is much less than the number of dofs in the model, N . The improved algorithm requires $O(a^2)$ operations, and is made even more efficient by using a sparse matrix formulation.

Again let M and K denote the $N \times N$ analytical mass and stiffness matrices of the system, respectively, and let ω_i denote the i^{th} measured frequency. We will assume that the i^{th} mode of the structure, call it ϕ_i , is measured at the a degrees of freedom $\{n(j)\}_{j=1, \dots, a}$, with $a \ll N$. The measured mode is further assumed to be corrupted by the noise vector $\eta \in \mathbb{R}^a$. Thus we have the measurement

model

$$\hat{\phi}_{ai} = E_a \phi_i + \eta$$

where E_a is the $a \times N$ matrix that selects the degrees of freedom $\{ \eta(j) \}$. We note that before we took $E_a = [I_a \ 0]$, which can always be assumed by a permutation of the physical coordinates. As we have seen previous] y, an effective way to extrapolate the measurement $\hat{\phi}_{ai}$ to the full mode is to solve the quadratic programming problem

$$\min_{\hat{\phi}_{Ni}} |(K - \omega_s^2 M) \hat{\phi}_{Ni}|^2, \quad \text{subject to} \quad |E_a \hat{\phi}_{Ni} - \hat{\phi}_{ai}|^2 \leq \epsilon, \quad (51)$$

where ϵ reflects the quality of the measurements. Typically ϵ is defined as a percentage of the square of the magnitude of the observed displacement $|\hat{\phi}_{ai}|$. In this brief note we will examine this problem a little more carefully, with an eye towards exploiting the property $a \ll N$.

To begin, let $\phi_{ext} \in \mathbb{R}^N$ denote any vector such that $E_a \phi_{ext} = \hat{\phi}_{ai}$. (For example forming ϕ_{ext} by appending zeros to $\hat{\phi}_{ai}$ will do.) Now let $\phi = \hat{\phi}_N - \phi_{ext}$, so that (1) can be rewritten as

$$\min_{\phi} |[K - \omega_s^2 M] (\phi + \phi_{ext})|^2, \quad \text{subject to} \quad |E_a \phi|^2 \leq \epsilon. \quad (52)$$

The solution to (51) is then realized as $\hat{\phi}_N = \phi + \phi_{ext}$ where ϕ is the solution to (52). It is straightforward to verify that the objective functional and constraints are both convex in (52), so that (52) is a convex programming problem. Because of the convexity, the Kuhn--Tucker (KT) necessary conditions for optimality are then also sufficient, and furthermore any local solution is also a global solution [16].

With this in mind we will investigate the KT conditions for this problem. First we form the Lagrangian, $L(\lambda, \phi)$, with λ a real number and

$$L(\lambda, \phi) = \langle (G + \lambda I_a) \phi, \phi \rangle + 2 \langle G \phi, \phi_{ext} \rangle - \lambda \epsilon + \langle G \phi_{ext}, \phi_{ext} \rangle, \quad (53)$$

where the $N \times N$ matrices G and I_a are defined as $G = [K - \omega^2 M] / 2$ and $I_a = E_a^T E_a$. The K'T conditions are:

$$\nabla_{\phi} L(\lambda, \phi) = 0, \quad (54a)$$

with

$$\lambda \geq 0, \quad (54b)$$

$$\epsilon - |E_a \phi|^2 \geq 0 \quad (54c)$$

and

$$\lambda [\epsilon - |E_a \phi|^2] = 0. \quad (54d)$$

Now (54a) is equivalent to

$$(G + \lambda I_a) \phi = -G \phi_{ext}. \quad (55)$$

Assuming G is invertible, (55) has a solution for any $\lambda \geq 0$ since $I_a \geq 0$ (In fact if $\lambda > 0$ it is sufficient that $N(G) \cap N(E_a) = \emptyset$; however we will assume that G is invertible.) The KT condition (54d) implies either $\lambda = 0$ or $\epsilon - |E_a \phi|^2 = 0$. If $\lambda = 0$, then $\phi = -\phi_{ext}$ and $\hat{\phi}_N = 0$. This can only happen if $\epsilon \geq |\phi_{ext}|^2$, which is an uninteresting choice of constraint. So we will assume that $\epsilon < |\phi_{ext}|^2$. In this

case the solution to the optimization problem is

$$\hat{\phi}_{Ni} = \phi_{ext} + \phi(\lambda), \quad (S6)$$

where

$$\phi(\lambda) = -(G + \lambda I_a)^{-1} G \phi_{ext} \quad (S7)$$

satisfies

$$|E_a \phi(\lambda)|^2 = \epsilon. \quad (S8)$$

We will now show that (58) is indeed satisfied for some $\lambda > 0$. Define $T(\lambda) = |E_a \phi(\lambda)|^2$. Observe under the present assumptions that $T(0) \geq \epsilon$. Also note that T is a continuous function. Since G is invertible there exists an invertible matrix X such that $F = X^T G X$ and $T = X^T I_a X$ are both diagonal with non-negative entries. Furthermore, since $\text{rank}(I_a) = a$, it follows that T has only a non-zero entries. By a permutation we can arrange these so that the non-zero entries occupy the first a rows of T . So now we can write

$$\phi(\lambda) = X \psi(\lambda),$$

where

$$\psi(\lambda) = -(F + \lambda T)^{-1} X^T G \phi_{ext}.$$

Let x_j denote the j^{th} column of X . Then we have

$$\begin{aligned} T(A) &= \langle I_a X \psi(\lambda), I_a X \psi(\lambda) \rangle \\ &= \langle X^T I_a X \psi(\lambda), \psi(\lambda) \rangle \\ &= \sum_{j=1}^a \left[\frac{T_j \langle x_j, G \phi_{ext} \rangle}{F_j + \lambda T_j} \right]^2. \end{aligned}$$

Thus it is seen that $\lim_{\lambda \rightarrow \infty} T(\lambda) = 0$. Hence by continuity there must exist a λ_0 such that $T(\lambda_0) \geq \epsilon$. This discussion is summarized in

Theorem 1. If G is invertible, the optimization problem (51) has a unique global solution $\hat{\phi}_{ai}$ obtained by solving equations (56)–(58) above. (57) has a unique solution of each λ , and there exists a unique λ_0 that solves (8) whenever $\epsilon < |\phi_{ext}|^2$. If $\epsilon \geq |\phi_{ext}|^2$ then $\hat{\phi}_N = 0$ solves (51).

Theorem 1 settles the question of existence, uniqueness, and how to obtain the solution to (1). We will next take up the question of *efficiently* solving this optimization problem. A cursory analysis of the problem seems to require finding the transformation X . In general X is a full $N \times N$ matrix. Obtaining X for large N is a very troublesome point. We will show how to circumvent this difficulty.

The relevant observation to make here is that simultaneously diagonalizing G and I_a is equivalent to obtaining the eigenvalues and eigenvectors of the matrix $Z = G \text{''} I_a$. Now let $R(Z)$ be the range of Z , where $R(Z) = R(G \text{''} E_a^T)$ has dimension u . This is the fact that we shall exploit. Let U be an orthogonal $N \times a$ matrix whose columns span $R(Z)$. If u is an eigenvector of Z with non-zero eigenvalue λ , it is evident that $u \in R(U)$ since $\lambda u = Z u \in R(Z) = R(U)$. Hence there exists $y \in \mathbb{R}^a$ such that $U y = u$. Let u_i denote the a independent eigenvectors of $G \text{''} I_a$ with non-zero eigenvalues, and for each i let $U y_i = u_i$. Let Y be the $a \times a$ matrix with columns y_i , and define $X_a = U Y$. Then it follows that

$$F_a = X_a^T G X_a,$$

and

$$T_a = X_a^T I_a X_a$$

are both $a \times a$ diagonal matrices. Essentially what we have accomplished here is the simultaneous diagonalization of G and I_a on the subspace spanned by U . It will next be shown that this is actually enough to solve (57)--(58).

introduce the orthogonal projections $P_U = UU^T$ and $P_V = I - P_U$. P_U is the orthogonal projection onto $R(U)$ and P_V is the complementary projection onto the orthogonal complement of $R(U)$. Since G is invertible, (55) is equivalent to

$$(I + \lambda Z) \phi(\lambda) = -\phi_{ext}. \quad (s9)$$

Now

$$\begin{aligned} Z &= (P_U + P_V) Z (P_U + P_V) \\ &= Z P_U + Z P_V, \end{aligned}$$

since $R(Z) = R(P_U)$. Writing $\phi(\lambda) = P_U \phi(\lambda) + P_V \phi(\lambda)$, (59) becomes

$$P_V \phi + P_U \phi + \lambda Z [P_V \phi + P_U \phi] = -P_V \phi_{ext} - P_U \phi_{ext}. \quad (60)$$

$R(P_V) \cap R(P_U) = O$ implies

$$P_V \phi = -P_V \phi_{ext}. \quad (61)$$

It remains to solve for $P_U \phi$. Substituting (61) into (60) and multiplying through by G , we obtain

$$(G + \lambda I_a) P_U \phi = -G P_U \phi_{ext} + \lambda I_a P_V \phi_{ext}. \quad (62)$$

Because $R(X_a) = R(P_U)$, there exists a vector $y \in \mathbb{R}^a$ such that $P_U \phi = X_a y$. Now we can reduce (62) via the transformation X_a

$$(X_a^T G X_a + \lambda X_a^T I_a X_a) y = X_a^T (-G P_U \phi_{ext} + \lambda I_a P_V \phi_{ext}), \quad (63)$$

to obtain

$$\begin{aligned} P_U \phi(\lambda) &= X_a y \\ &= X_a (F_a + \lambda T_a)^{-1} X_a^T (-G P_U \phi_{ext} + \lambda I_a P_V \phi_{ext}). \end{aligned} \quad (64)$$

Thus we obtain the final result

$$\phi(\lambda) = X_a (F_a + \lambda T_a)^{-1} X_a^T (-G P_U \phi_{ext} + \lambda I_a P_V \phi_{ext}) - P_V \phi_{ext}. \quad (65)$$

with $P_U \phi(\lambda)$ computed from (64) above.

Once the matrix X_a , and the vectors F_a and T_a are obtained, the computation of (64) for any λ requires $O(na)$ flops, while $T(\lambda) = |E_a \phi(\lambda)|^2$ is determined in just $O(a^2)$ flops. Thus, computing T is very cheap, and it becomes a straightforward matter to solve $T(\lambda) = \epsilon$. As we saw earlier T decreases

monotonically to zero. A simple solution method we have implemented is to increase λ exponentially until $T(A) < \epsilon$ to obtain an initial interval containing the solution. Once this interval is determined a bisection method is implemented.

The most expensive computation involved in determining X_a when $N \gg a$ is computing the transformation Z . For full matrices this is an $O(N^3)$ operation. Fortunately, in structures applications this computation can be reduced considerably by utilizing sparse matrix techniques.

7.0. FURTHER RESULTS AND CONCLUDING REMARKS

Several mode shape expansion methods have been proposed and investigated, These expansion techniques fall into three main categories. The first one uses direct solutions of the static and dynamic equations to obtain a closed-form equation. This category includes the Guyan and the Kidder methods. It is shown that these direct methods can also be written in terms of a constrained minimization problem. The second category uses a least-squares method to minimize the error between the measured and modeled eigenvectors. Within this category, the Procrustes method imposes orthogonality of the mode shapes. The third category formulates the expansion as a least-squares minimization problem with "soft constraint". One approach incorporates the soft constraint as a penalty term; a second approach uses an inequality constraint. These constraints can depend on either the measured or an already expanded mode shape.

The trade study demonstrated that the LSQI method based on minimization of the dynamic force equation and subject to bounds imposed by measurement noise has the best performance. The Procrustes method has an average performance, whereas the direct methods are the worst, The LSQI methods based on strain energy minimization yield results comparable to the Guyan or Kidder methods, even in the presence of large measurement noise, and without any computational advantage.

It was shown that the Guyan method can only properly expand the first few modes. To get a suitable expansion with the Guyan method, a minimum ratio of 3 to 4 accelerometers per mode is required - as commonly practiced experimentally. Lower ratios of instrumented dofs to modes and better performance can be achieved with the Procrustes, the Kidder and the LSQ13. Under ideal experimental and analytical conditions, the Kidder method can correctly expand all modes represented in the data set. This method is not sensitive to the asset selection, but is extremely sensitive to noise and model deficiencies. It was shown that the LSQI methods based on strain energy minimization did not improve on the accuracy of the direct methods, while imposing a significant computational cost. Computationally, the most efficient expansion method is the Procrustes method. Along with the LSQ13 method, it is the only method which can properly expand mode shapes which are not completely represented in the selected instrument locations. However, the Procrustes method can only achieve this if the analytical and experimental modes are properly paired. Pairing is automatically guaranteed in the other methods through the FEM model and the measured modal frequencies. Furthermore, the Procrustes method is very sensitive to measurement dof location and selection, as well as to the number of simultaneously expanded modes, In an actual situation this is a big disadvantage as the real solution is not known, and the variation in the error can be great,

The LSQI expansion method with dynamic force minimization has the best all-around performance. It is insensitive to moderate amounts of measurement error, and is capable of predicting eigenvectors at unmeasured dofs with greater accuracy than the noise-corrupted data measured at those locations. LSQI3 is the only method which is capable of regularizing global and local model errors, resulting in mode shapes of higher accuracy than the model originally predicted, even in the presence of experimental noise. This makes the LSQI expansion method with Dynamic Force Minimization ideally suited for recursive model updating, damage detection and response prediction technique. Its biggest disadvantage is in its computational requirements, however, with improved algorithms and more powerful computers (e. g., parallel processing), this is not a significant issue.

REFERENCES

1. G.I.I. Golub and C.F. Van Loan, *Matrix Computations*, John Hopkins Univ. Press, Baltimore, MD, 1983.
2. R.J. Guyan, "Reduction of Stiffness and Mass Matrices", *AIAA Journal*, Vol. 3, No. 2, 1965,
3. R.I. Kidder, "Reduction of Structural Frequency Equations", *AIAA Journal*, Vol. 11, No. 6, June 1973.
4. S.W. Smith and CA. Beattie, "Simultaneous Expansion and Orthogonalization of Measured Modes for Structure Identification", Proc. AIAA Dynamics Specialist Conference, Long Beach, Ca., April 1990.
5. T.G. Carrie, R. I. Mayes, and M.B. Levine-West, "A Modal Test of a Space-Truss for Structural Parameter Identification", Proc. of the 11th International Modal Analysis Conf., Kissimmee, Fl., Feb 1993.
6. J.R. Red-Horse, E.L. Marek, and M.B. Levine-West, "System Identification of the JPL Micro-Precision Interferometer Truss: Test-Analysis Reconciliation, Proc. of the 34th SDM Conf., La Jolla, Ca., April 1993.
7. Kammer, D. C., "Test-Analysis Model Development Using an Exact Modal Reduction", International Journal of Analytical and Experimental Modal Analysis, Ott, 1987
8. Neat, G. W., L.F. Sword, B.E. Hines, and R.J. Calvet, "Micro-Precision Interferometer Testbed: End-To-End System Integration of Control Structure Interaction Technologies", Proceedings of the SPIE Symposium OE/Aerospace. Science and Sensing, Conference on Spaceborne Interferometry, Orlando, FL, April 1993.
9. Imregun, M., and D. J. Ewins, "An Investigation Into Mode Shape Expansion Techniques", Proc. of the 11th International Modal Analysis Conf., Kissimmee, Fl., Feb 1993, pp. 168-175, Vol. 1.
10. O'Callahan, J., "A Procedure for an Improved Reduced System (IRS) Model", Proc. of the 7th international Modal Analysis Conf., Las Vegas, Nev., 1989.
11. Baker, M. "Review of Test/Analysis Correlation Methods and Criteria for Validation of Finite Element Models for Dynamic Analysis", Proc. of the 10th International Modal Analysis Conf., San Diego, Ca., Feb. 1992, pp. 984-990.
12. Kim, H., and H. Doiron, "Modal Identification Experiment Design for Large Space Structures",

Paper No. 91-1183, Proc. AIAA 32nd SDM conf., Baltimore Md., April 9-10, 1991,

13. Karnmer, D. C., "A Hybrid Approach to Test Analysis Model Development for LSS", J. of Vibrations and Acoustics, July 1991, Vol. 113, pp. 325-332.

14. O'Callahan, J., P. Avitabile, and R. Riemer. "System Equivalent Reduction Expansion Process (SEREP)", 7th International Modal Analysis Conf., Las Vegas, Nev., Feb. 1989.

1s. G. Lallement, and S. Cognan, "Matching Finite Element Models to Modal Data," International Conf. Spacecraft Struc. and Mech. Testing, ESTEC, Noordwijk, NL., April 1991.

Mode #	Freq (Hz)	ΔF (%)	$\Delta \phi$ (%)	Model MAC	Test MX
1	7.67	1.00	5.64	1.00	1.00
2	11.43	1.90	7.12	0.99	1.00
3	12.47	1.54	6.33	1.00	1.00
4	27.38	6.73	8.54	0.99	1.00
5	32.80	3.68	31.26	0.90	0.9s
6	34.23	8.33	36.94	0.86	0.93
7	38.52	8.83	24.47	0.94	0.97
8	44.59	3.14	30.19	0.91	0.9s
9	46.99	5.07	39.38	0.84	0.92

Table I. MPI Pre-Test Model: Frequency Error, Mode Shape Error, MAC (Eq.46) and MX (Eq. 49) with Respect to Test Data.

Mode #	Freq (Hz)	ΔF (%)	$\Delta \phi$ (%)	Model MAC	Test MX
1	7.67	1.00	5.64	1.00	1.00
2	11.43	1.90	7.12	0.99	1.00
3	12.47	1.54	6.33	1.00	1.00
4	27.38	6.73	8.54	0.99	1.00
5	32.80	3.68	31.26	0.90	0.95
6	34.23	8.33	36.94	0.86	0.93
7	38.52	8.83	24.47	0.94	0.97
8	44.59	3.14	30.19	0.91	0.95
9	46.99	5.07	39.38	0.84	0.92

Table II MPI Pre-Test Model: Frequency Error, Mode Shape Error, MAC (Eq.46) and MX (Eq. 49) With Respect to Test Data.

Mode #	Freq (Hz)	ΔF (%)	$\Delta \phi$ (%)	Test MAC	Test MX
1	7.82	0.88	5.70	1.00	1.00
2	11.66	0.11	8.26	0.99	1.00
3	12.75	0.67	7.42	0.99	1.00
4	29.32	0.56	6.71	1.00	1.00
5	34.45	1.16	6.04	1.00	1.00
6	37.76	1.12	9.82	0.99	0.99
7	42.81	1.32	9.61	0.99	1.00
8	47.30	2.74	15.18	0.98	0.99
9	51.14	3.30	26.88	0.93	0.96

Table 111 MPI Updated Model: Frequency Errors, Mode Shape Error (Eq. 44), MAC (Eq. 46) And MX (Eq. 49) With Respect To Test Data.

ASET #	NUMBER OF INSTRUMENTS	LOCATION CRITERIA
1	3	1 per boom tip
2	12	triax@ boom tips
3	12	optimal MAC
4	6	best mode 1&2
5	6	2 per boom tips

Table IV Summary of Instrument Location Cams.

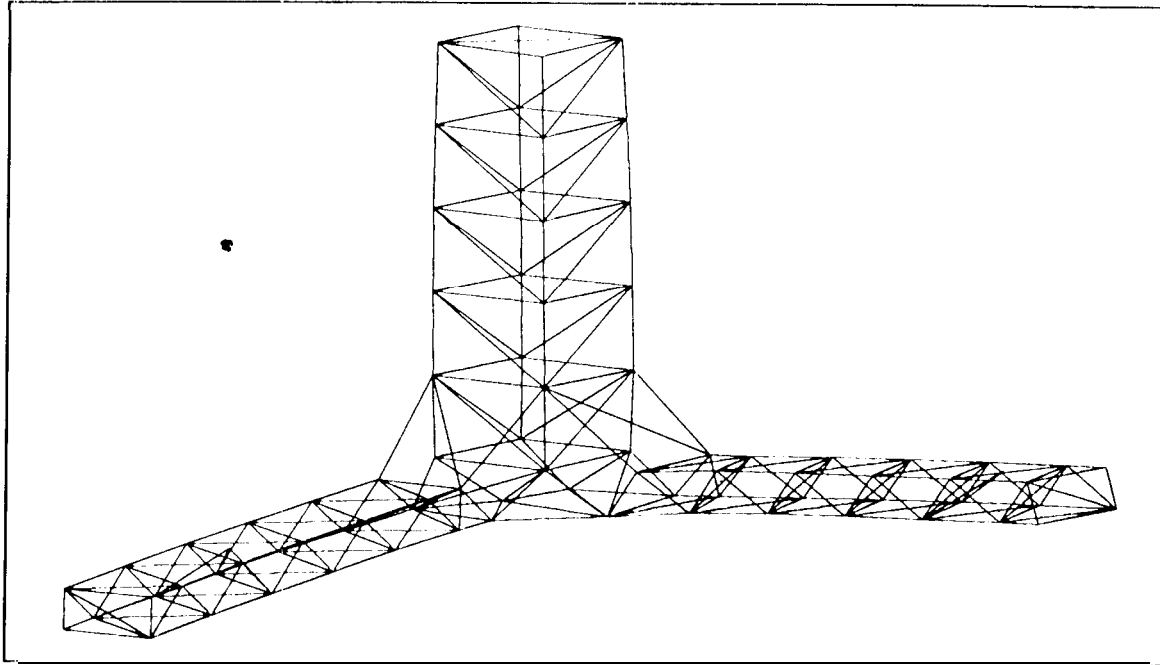


Figure 1 The Micro-Precision Interferometer Testbed.

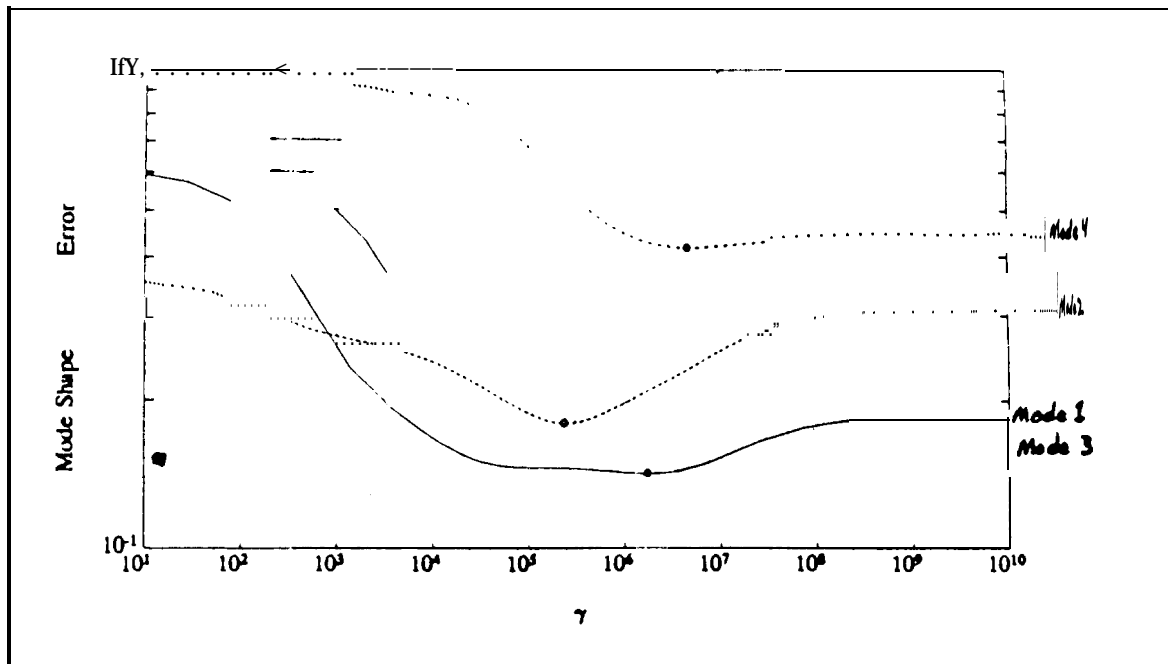


Figure 2 Mode Shape Error as a Function of Weighting Coefficient γ for the Strain Energy Expansion Method with Measurement Error Penalty.

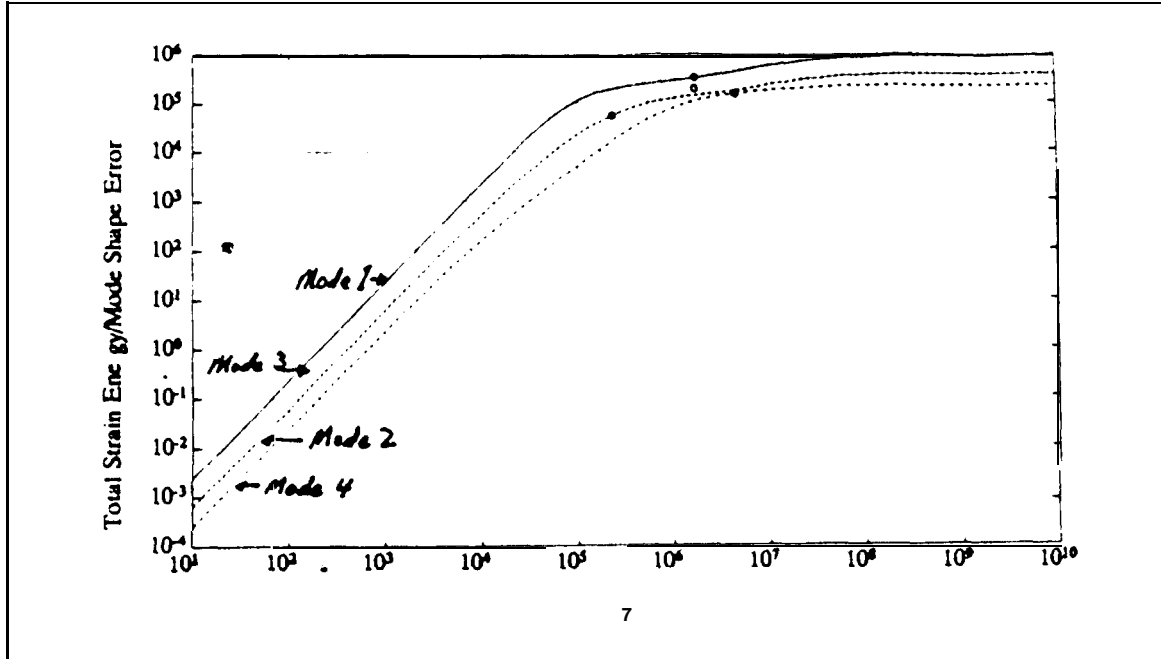


Figure 3 Mode Shape Error as a Function of Weighting Coefficient γ for the Strain Energy Expansion Method with Measurement Error Penalty.

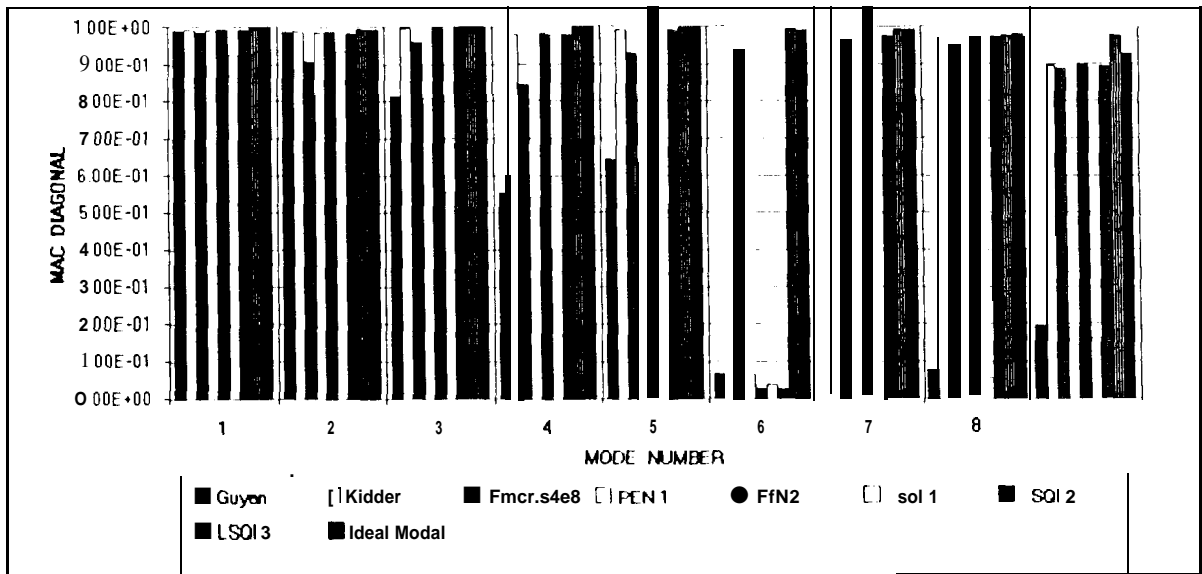


Figure 4 MAC Diagonal (measured vs expanded) - Expansion from 12 dofs (aset5) to 240 dofs with ideal model and no additional measurement error.

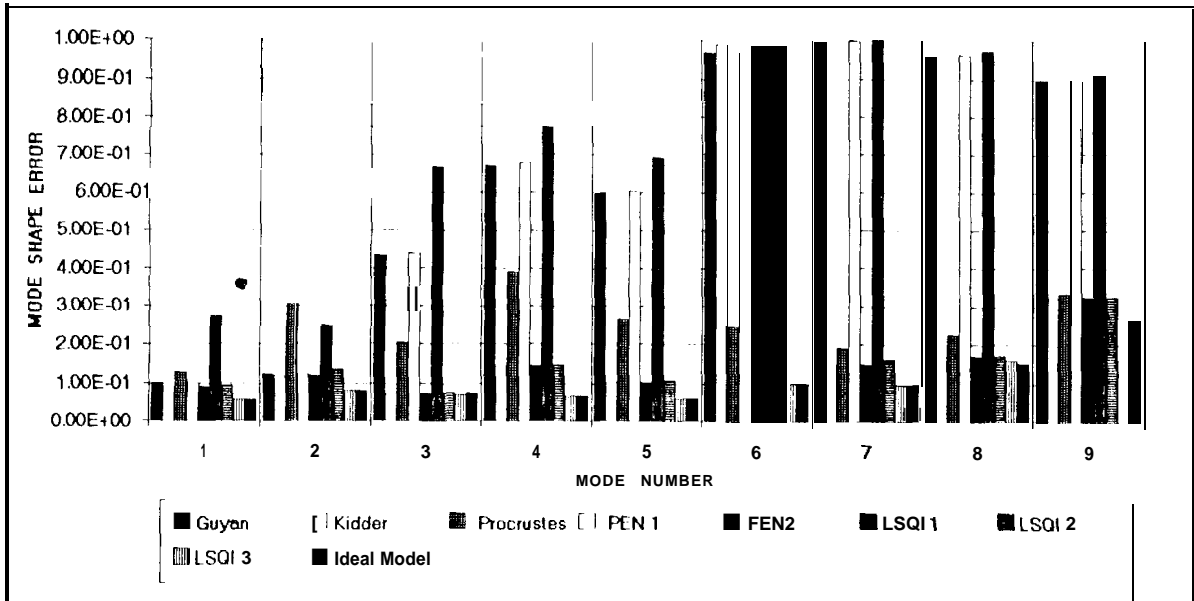


Figure 5 Frobenius Norm Mode Shape Error (measured vs expanded) - Expansion from 12 dofs (aset5) to 240 dofs with ideal model and no additional measurement error.

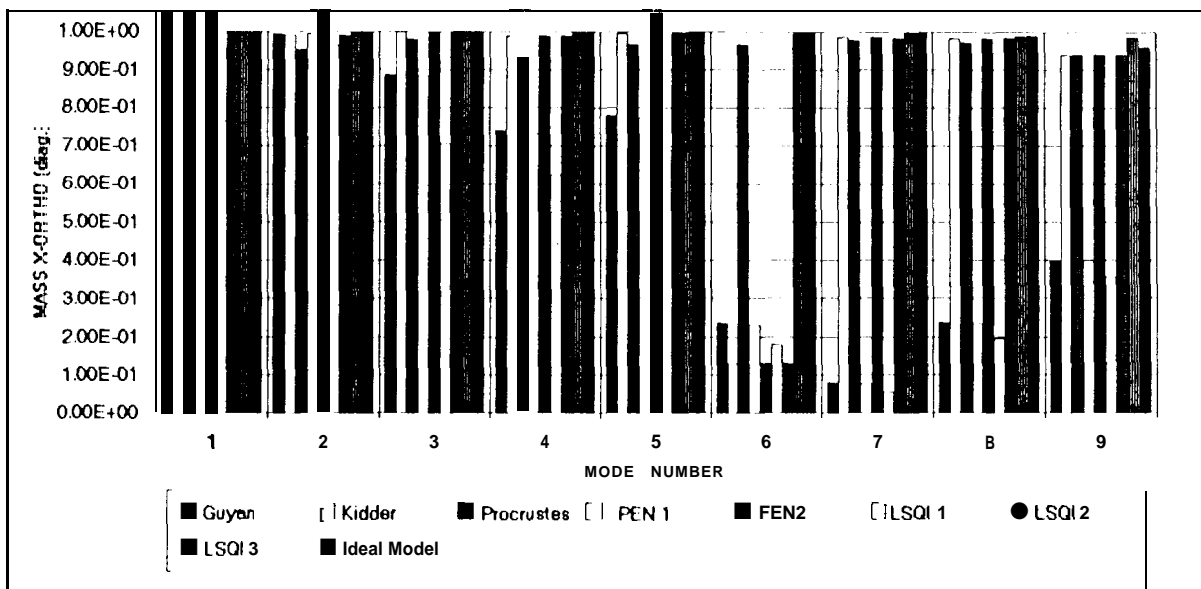


Figure 6 MX Diagonal (measured vs expanded) - Expansion from 12 dofs (aset5) to 240 dofs with ideal model and no additional measurement error.

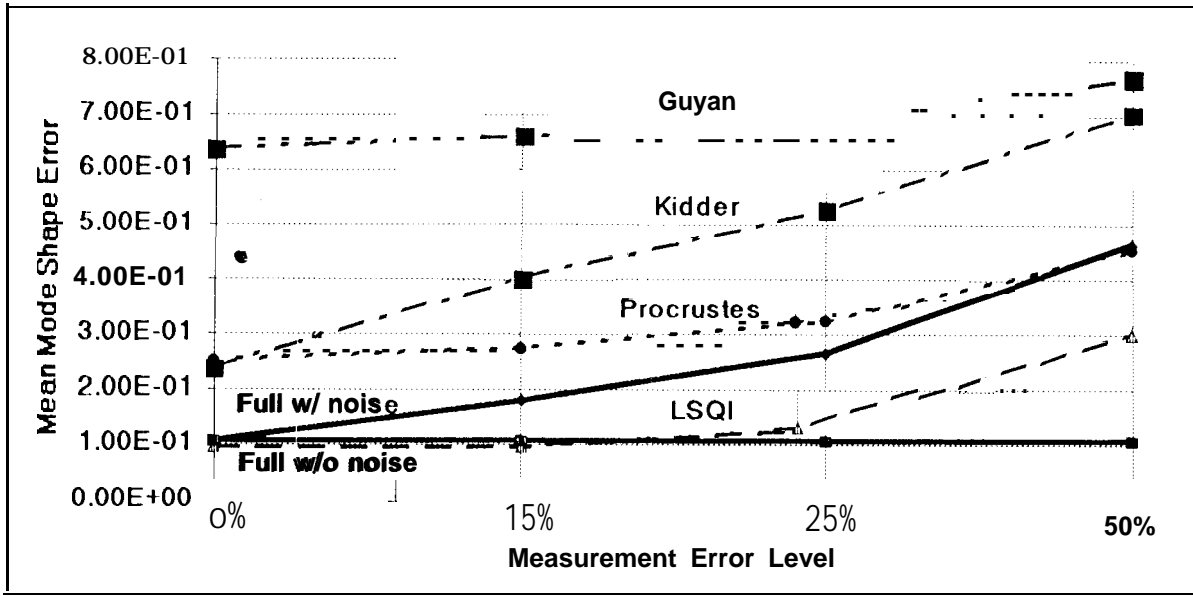


Figure 7 Mean mode shape error as a function of measurement noise - Expansion of nine modes from 12 dofs (aset5) to 240 dofs with updated FEM model.

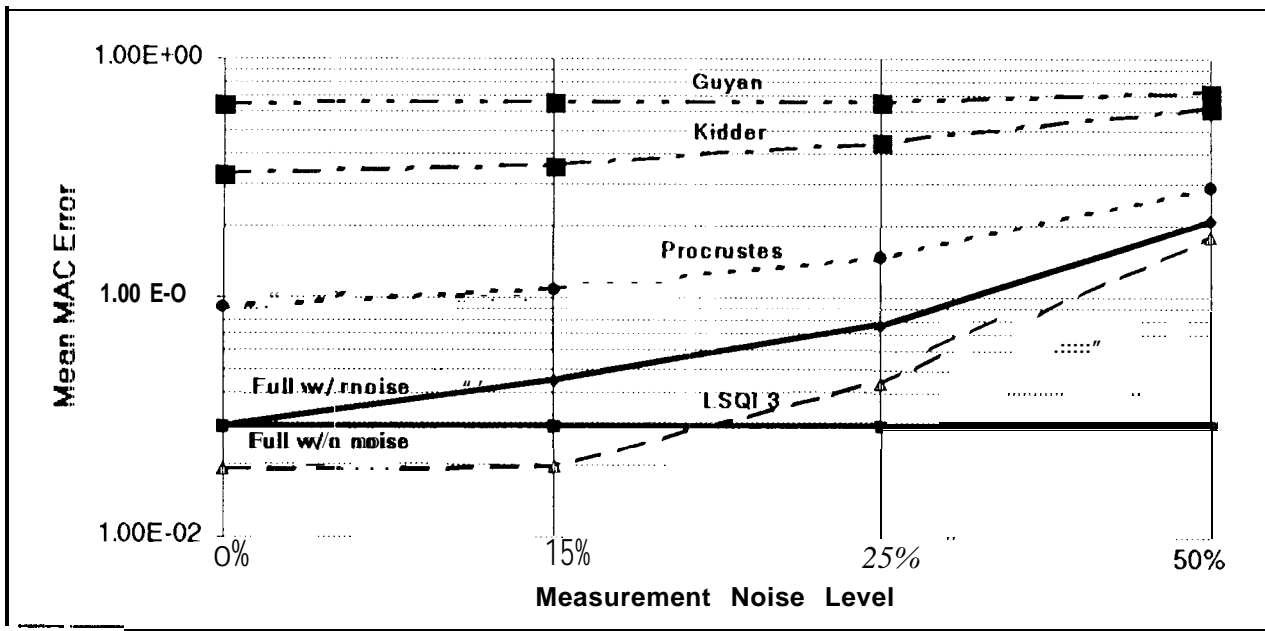


Figure 8 Mean MAC error as a function of measurement noise - Expansion of nine modes from 12 dofs (aset5) to 240 dofs with updated FEM model.

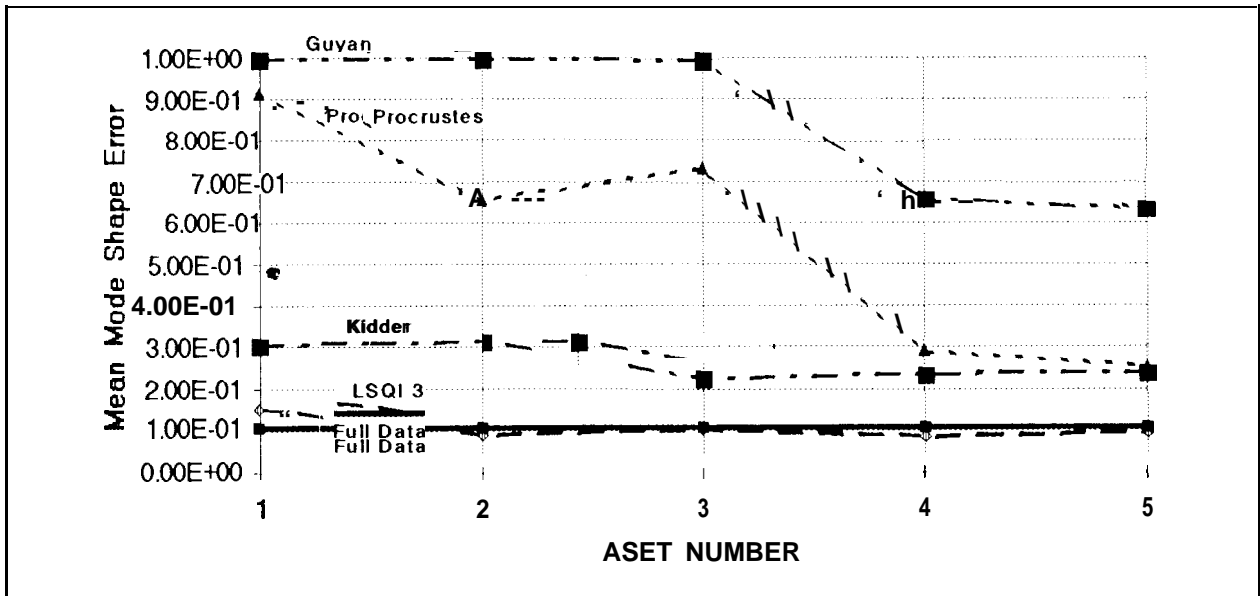


Figure 9 Mean mode shape error as a function of *aset* selection - Expansion of nine modes to 240 dofs with updated FEM model and no additional measurement noise.

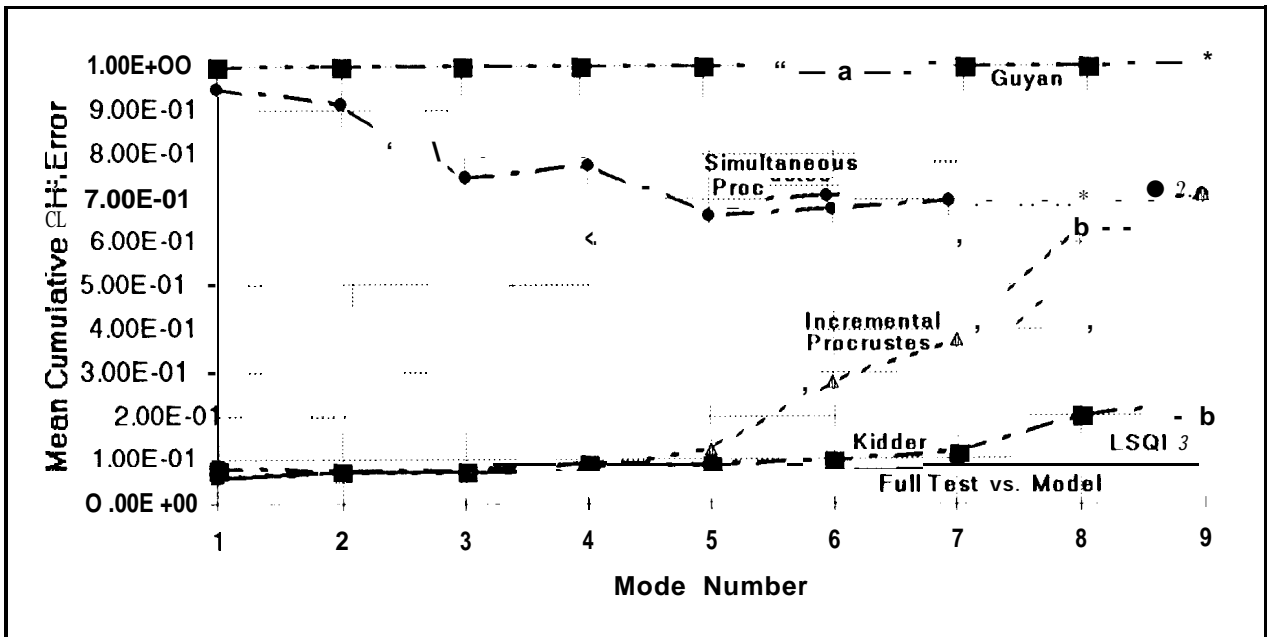


Figure 10 Mean cumulative mode shape error - Expansion from 6 dofs (*aset3*) to 240 dofs with updated FEM model and no additional measurement noise.

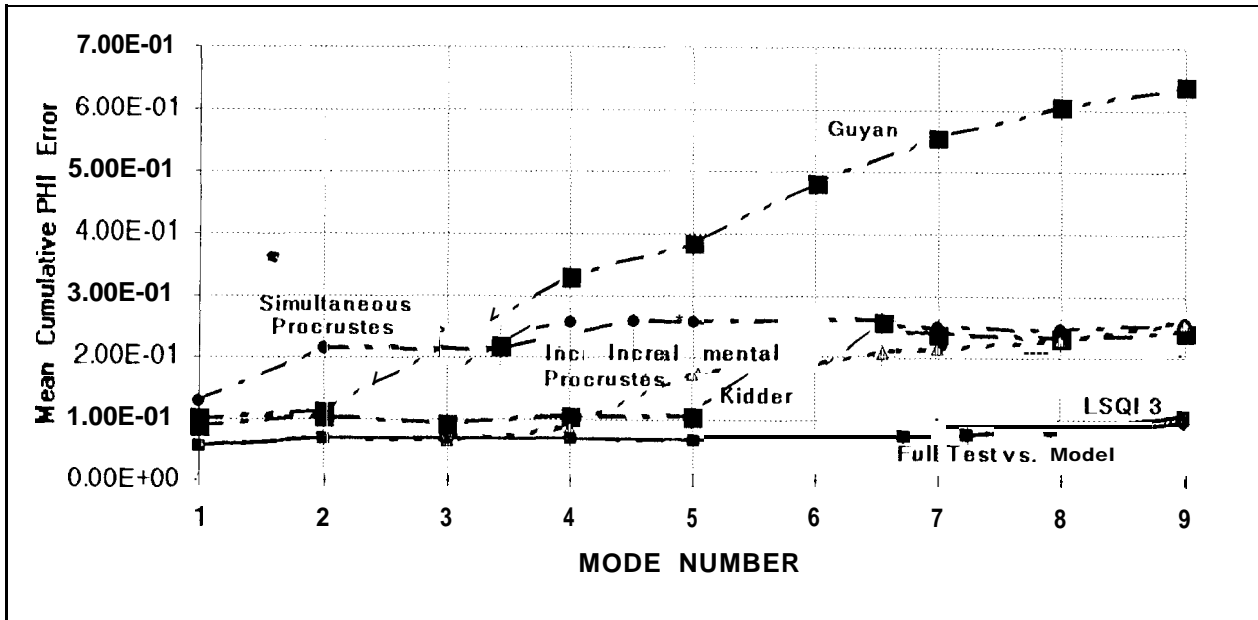


Figure 11 Mean cumulative mode shape error - Expansion from 12 dofs (*aset5*) to 240 dofs with updated FEM model and no additional measurement noise.

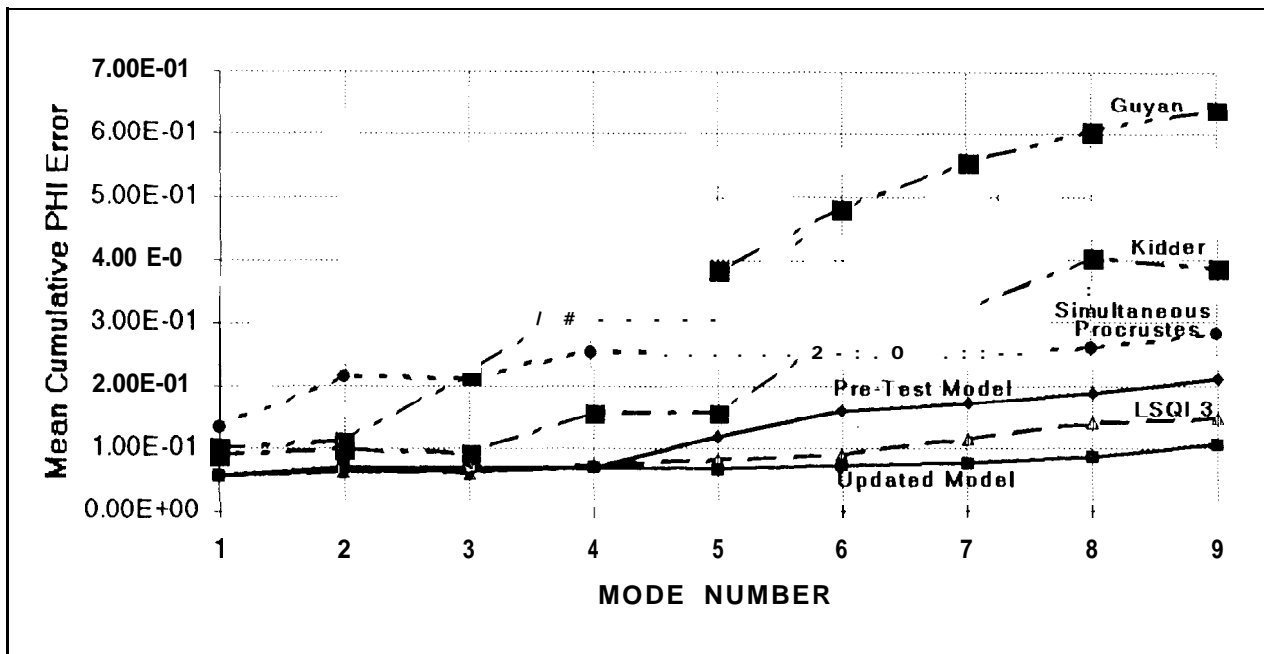


Figure 12 Mean cumulative mode shape error - Expansion from 12 dofs (*aset5*) to 240 dofs with pre-test FEM model and no additional measurement noise.

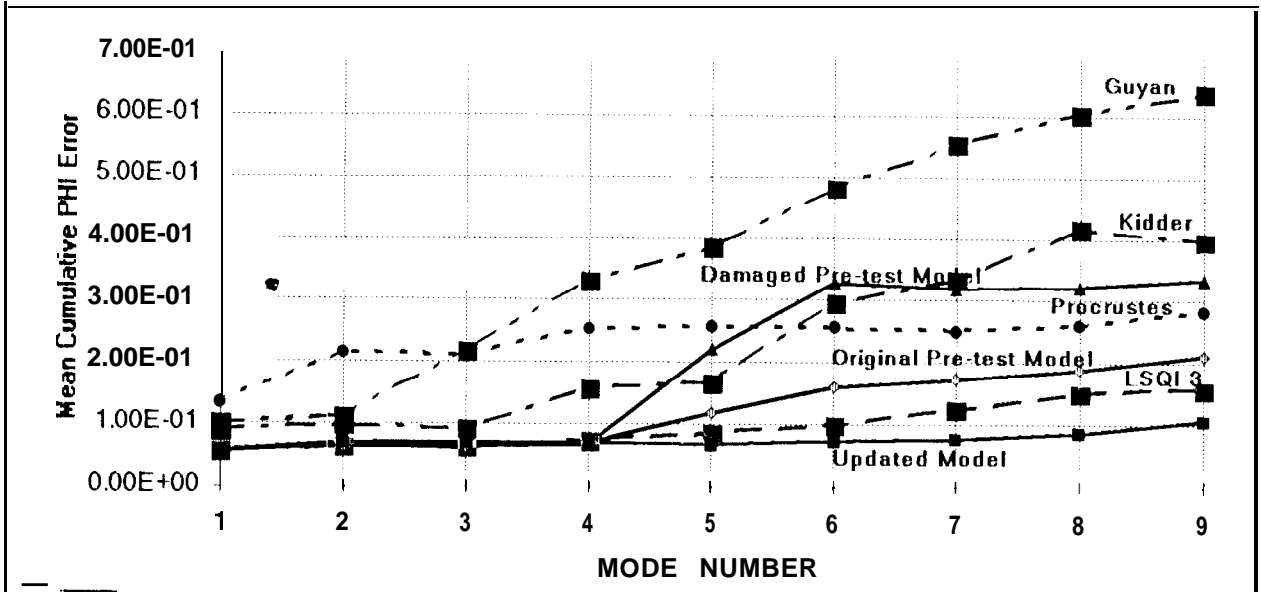


Figure 13 Mean cumulative mode shape error - Expansion from 12 dofs (*aset5*) to 240 dofs with damaged pre-test FEM model and no additional measurement noise.

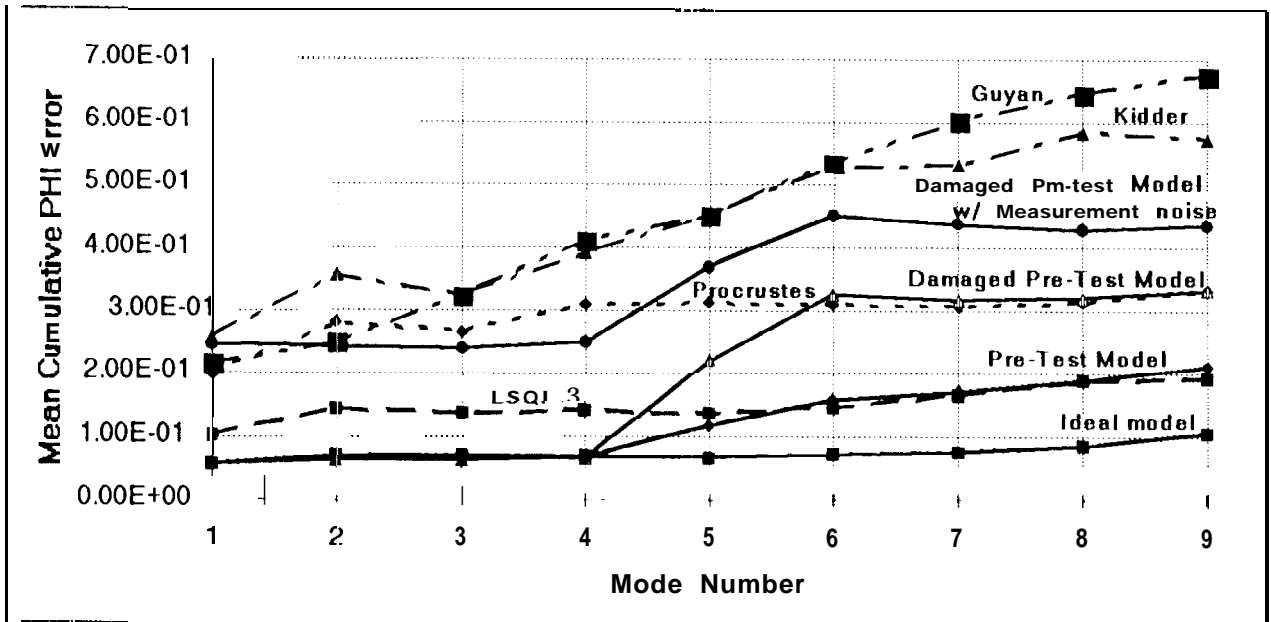


Figure 14 Mean cumulative mode shape error - Expansion from 12 dofs (*aset5*) to 240 dofs with damaged pre-test FEM model and 2S% additional measurement noise.